THE JOURNAL OF PHYSICAL CHEMISTRY B
A JOURNAL OF THE AMERICAN CHEMICAL SOCIETY

pubs.acs.org/JPCB

Article

Modulation of the Directionality of Hole Transfer between the Base and the Sugar-Phosphate Backbone in DNA with the Number of Sulfur Atoms in the Phosphate Group

Sergey A. Denisov, Samuel Ward, Viacheslav Shcherbakov, Alexander D. Stark, Renata Kaczmarek, Ewa Radzikowska-Cieciura, Dipra Debnath, Taisiya Jacobs, Anil Kumar, Michael D. Sevilla, Pascal Pernot, Roman Dembinski,* Mehran Mostafavi,* and Amitava Adhikary*

Cite This: *J. Phys. Chem. B* 2022, 126, 430−442

Read Online

ACCESS | Metrics & More | Article Recommendations | Supporting Information

ABSTRACT: This work shows that S atom substitution in phosphate controls the directionality of hole transfer processes between the base and sugar-phosphate backbone in DNA systems. The investigation combines synthesis, electron spin resonance (ESR) studies in supercooled homogeneous solution, pulse radiolysis in aqueous solution at ambient temperature, and density functional theory (DFT) calculations of in-house synthesized model compound dimethylphosphorothioate (DMTP(O^-)=S) and nucleotide (5′-*O*-methoxyphosphorothioyl-2′-deoxyguanosine (G−P(O^-)=S)). ESR investigations show that DMTP(O^-)=S reacts with $Cl_2^{\bullet-}$ to form the $\sigma^2\sigma^{*1}$ adduct radical −P−S∴Cl, which subsequently reacts with DMTP(O^-)=S to produce [−P−S∴S−P−]$^-$. −P−S∴Cl in G−P(O^-)=S undergoes hole transfer to Gua, forming the cation radical ($G^{\bullet+}$) via thermally activated hopping. However, pulse radiolysis measurements show that DMTP(O^-)=S forms the thiyl radical (−P−S$^\bullet$) by one-electron oxidation, which did not produce [−P−S∴S−P−]$^-$. Gua in G−P(O^-)=S is oxidized unimolecularly by the −P−S$^\bullet$ intermediate in the sub-picosecond range. DFT thermochemical calculations explain the differences in ESR and pulse radiolysis results obtained at different temperatures.

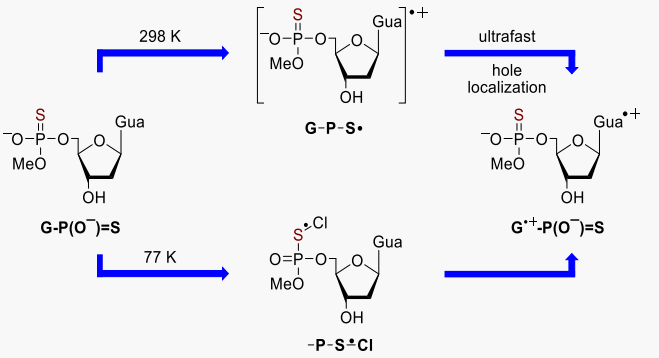

1. INTRODUCTION

The interaction of DNA with ionizing radiation results in instantaneous random ionization events both within the DNA bases and the sugar-phosphate backbone that lead to the creation of sites of electron loss (i.e., hole or cation radical) and an ejected electron. Subsequent random trapping of these excess electrons by bases and the sugar-phosphate backbone in irradiated DNA forms transient anion radical sites.[1−13]

Electron spin resonance (ESR) spectroscopic studies on the analysis of cohort of trapped radicals in irradiated (irradiated at 4 K or at 77 K) DNA oligomers and in irradiated (irradiated at 77 K) hydrated (Γ = number of water molecules/nucleotide = 12 ± 2) DNA have shown that the holes localize on the most electropositive base, guanine, and the excess electron localizes on the electron-affinic bases, thymine and cytosine. Thus, these studies provide the evidence of both hole and electron transfer[1−10,13] and are of great significance regarding the ultimate location of DNA damage that lead to cell death, mutations, and aging.[10−16]

Hole formation on the bases and on the sugar-phosphate backbone upon ionization happens in proportion to the electron density at that site.[1,2,5−8,17−21] We note here that extensive work has focused on the hole transfer processes in DNA because it is thought to be the major damaging entity.[1−13] The hole localization at the guanine base in irradiated DNA occurs via direct ionization and base-to-base and backbone-to-base hole transfer processes.[1,2,5−8,17−23]

The rate and extent of hole transfer from the sugar-phosphate backbone to the bases, from the bases to the sugar-phosphate backbone and from phosphate to sugar in the backbone determine the yield of sugar radicals.[5,6,17−31]

In phosphorothioates (Scheme 1), a sulfur atom is introduced in place of a nonbridging oxygen in the phosphate moiety, and this substitution decreases the ionization potential of phosphorothioates relative to an unmodified phosphate in DNA model compounds (monomers and oligomers).[5,6,18,20] As a result, the lifetime of the hole on the sugar-

Received: October 19, 2021
Revised: November 19, 2021
Published: January 6, 2022

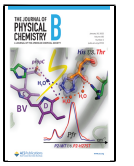

https://doi.org/10.1021/acs.jpcb.1c09068
J. Phys. Chem. B 2022, 126, 430−442

Scheme 1. Isolation of the Backbone-to-Base Hole Transfer Process Using Phosphorothioate

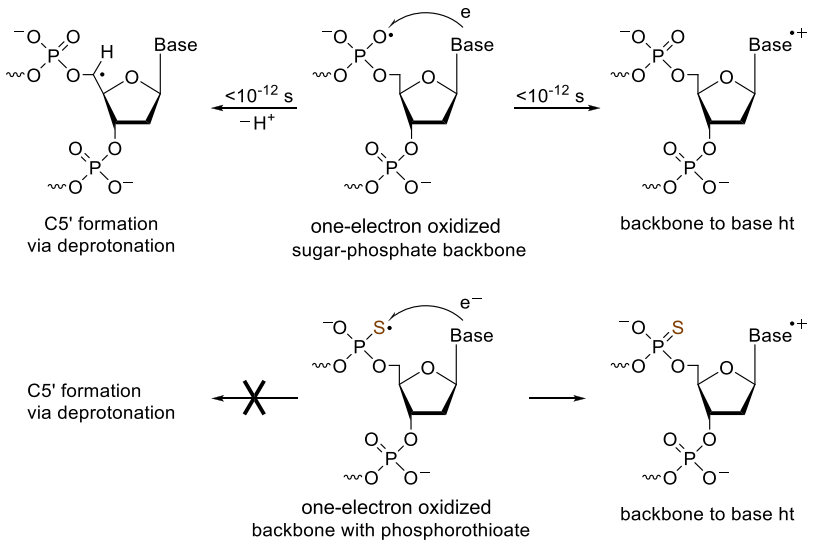

phosphorothioate backbone increases and allows for direct probing of only the backbone-to-base hole transfer processes without the competing sugar radical formation via deprotonation by ESR spectroscopy (Scheme 1).[5,6,18,20]

Our previous ESR spectroscopic investigations employing phosphorothioate-incorporated DNA oligomers (S-oligomers) and the phosphorothioate model compound diisopropyl phosphorothioate (DIP, Figure 1) along with density functional theory (DFT) calculations established that the addition of $Cl_2^{\bullet-}$ to DIP and to the S-oligomers led to the two-center three-electron $\sigma^2\sigma^{*1}$-bonded adduct radical (−P−S∴Cl) formation (Scheme 2).[18] For guanine-containing double-stranded (ds) S-oligomers containing only one phosphorothioate, P−S∴Cl caused one-electron oxidation of guanine base via thermally activated hopping but not of A, C, or T; thus, P−S∴Cl led to selective hole transfer to only G base (Scheme 2).[18] Based on these ESR studies and DFT calculations, the redox potential of P−S∴Cl was bracketed between those of G and A base moieties.[18] Furthermore, employing AT S-oligomers with multiple phosphorothioates, for example, d[ATATAsTsAsT]$_2$, our ESR studies showed that −P−S∴Cl reacts with a neighboring parent phosphorothioate to form the $\sigma^2\sigma^{*1}$-bonded disulfide anion radical ([−P−S∴S−P−]$^-$).[18]

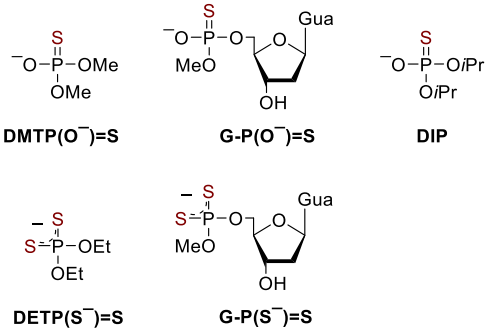

Figure 1. Chemical structures of compounds mentioned in this work: dimethylphosphorothioate (DMTP(O$^-$)=S), 5′-*O*-methoxyphosphorothioyl-2′-deoxyguanosine (G−P(O$^-$)=S), ammonium *O*,*O*′-diethyl dithiophosphate (DETP(S$^-$)=S), 5′-*O*-methoxyphosphorodithioyl-2′-deoxyguanosine (G−P(S$^-$)=S), and diisopropyl phosphorothioate (DIP).

When the second nonbridging O atom was replaced with another S atom in the phosphate moiety (phosphorodithioate, Figure 1), the ionization potential was found to decrease even lower than that of G$^{\bullet+}$ in 2′-deoxyguanosine-5′-monophosphate (5′-dGMP).[20] Neither the model compound for these phosphorodithioates [DETP(S$^-$)=S, Figure 1] nor the phosphorodithioate-modified 5′-dGMP (5′-*O*-methoxyphosphorodithioyl-2′-deoxygaunosine, G−P(S$^-$)=S, Figure 1) showed the $\sigma^2\sigma^{*1}$-bonded −P−S∴Cl adduct radical formation.[20] Instead, the dithiyl radical, P−2S$^{\bullet}$, was immediately formed and a thermally activated hole transfer from G$^{\bullet+}$ to the phosphorodithioate was found to occur unimolecularly, creating more P−2S$^{\bullet}$, as confirmed by ESR in glassy systems

Scheme 2. A $\sigma^2\sigma^{*1}$ Bonded −P−S∴Cl Radical Is Formed When the S-Oligomer and Also Phosphorothioate Model Compound, Dip, Interact with the $CL_2^{\bullet-}$.[18] The −P−S∴Cl Radical then Accepts an Electron from the Base Forming a Cl$^-$ and a Base (Guanine) Containing a Hole (Base (Guanine) Cation Radical, or G$^{\bullet+}$).[18]

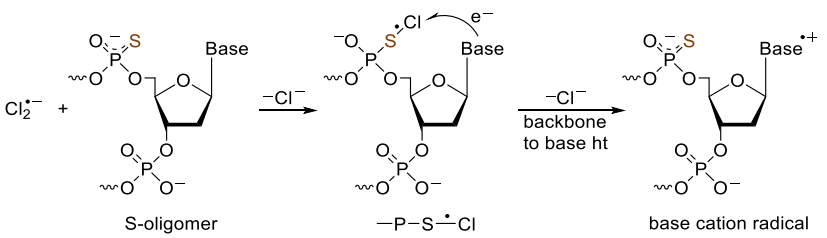

https://doi.org/10.1021/acs.jpcb.1c09068
J. Phys. Chem. B 2022, 126, 430−442

Scheme 3. Synthesis of Phosphorothioate, G−P(O⁻)=S Na⁺

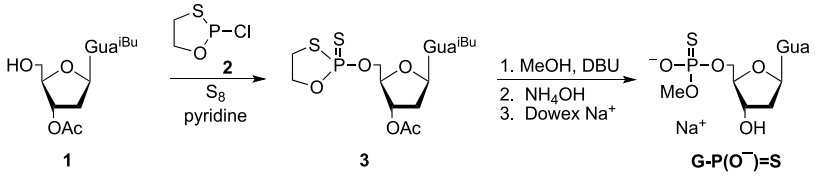

at low temperature, pulse radiolysis in aqueous solution at ambient temperature, and by DFT calculations. ESR showed that P−2S• underwent a bimolecular dimerization to form the $\sigma^2\sigma^{*1}$-bonded disulfide anion radical ([−P−2S∴2S−P−]⁻), though this anion radical was not observed by pulse radiolysis.[20] Contrary to the backbone-to-base hole transfer observed in phosphorothioates (Scheme 2),[18] neither the [−P−2S∴2S−P−]⁻ nor the P−2S• oxidized guanine and only the base-to-backbone hole transfer process was observed in phosphorodithioates.[20]

Apart from elucidation of the charge transfer processes between backbone and base studied here, DNA model systems (nucleotides and oligonucleotides of defined sequences) with either phosphorothioate or phosphorodithioate substitutions are widely employed as antisense nucleotides, owing to their good cellular uptake due to better nuclease stability.[32−35] In fact, phosphorothioation has been one of the first backbone modifications introduced.[34] It is noteworthy that either phosphorothioate or phosphorodithioate modification minimally affects the DNA geometry and base stacking.[18,20,34] Furthermore, phosphorothioation of the backbone is known to occur in nature and has been observed in bacteria and archea.[35,36]

Employing synthesis of the phosphorothioate model compound dimethyl phosphorothioate (DMTP(O⁻)=S, Figure 1) and of the 5′-nucleotide having guanine base (G−P(O⁻)=S, Figure 1) as well as combining ESR spectroscopy, pulse radiolysis, and DFT calculations in this work, we have sought answers to the following questions:

- As with our previous work on phosphorothioates[18] and phosphorodithioates,[20] do we observe P−S∴Cl formation in DMTP(O⁻)=S and G−P(O⁻)=S both at low temperature and at room temperature?
- Are the ESR parameters [e.g., hyperfine coupling constant (HFCC) values, *g*-values] of P−S∴Cl and [−P−S∴S−P−]⁻) radicals from DIP[18] and from DMTP(O⁻)=S affected by the substituting groups (isopropyl in DIP vs methyl in DMTP(O⁻)=S)?
- Following the previous work from our laboratory on the backbone-to-base on hole transfer in S-oligomers, would P−S∴Cl be able to oxidize the G base in G−P(O⁻)=S unimolecularly?
- Employing picosecond pulse radiolysis, would it be possible to obtain the timescale of the backbone-to-base hole transfer process in G−P(O⁻)=S in an aqueous solution at room temperature?
- Considering the results of this work employing G−P(O⁻)=S and our previous studies on phosphorothioate[18] and phosphorodithioate,[20] does the number of substitutions of the O atom by S atom in the phosphate control the direction of transfer of the hole and its localization between base and backbone?
- What is the biological significance/implication of these results?

2. EXPERIMENTAL SECTION

The compounds used in this work and the methodologies of synthesis, ESR spectroscopic studies, pulse radiolysis, and DFT calculations are presented in the supporting information along with references.

3. RESULTS AND DISCUSSION

3.1. Organization of the Results. This article reports the one-electron oxidation of phosphorothioates and extends our previous work on phosphorodithioate.[20] It presents a combination of synthesis, ESR spectroscopic studies, pulse radiolysis, and DFT calculations. Results obtained from these investigations and their relevant discussions are presented below.

3.2. Synthesis. *3.2.1. Synthesis of G−P(O⁻)=S Na⁺.* The investigated nucleotide G−P(O⁻)=S was prepared by introducing the thiophosphorane group using the oxathiaphospholane methodology, which was developed by Stec et al. for the stereocontrolled synthesis of phosphorothioate oligonucleotides.[37] This general route is applicable to the phosphorylation and thiophosphorylation of nucleosides and amino acids.[38−40] First, 3′-acyl-protected dGuo (**1**)[41] was combined with chlorooxathiaphospholane[42] (**2**; Scheme 3). The subsequent tricoordinate phosphorus intermediate (not illustrated and not isolated) was treated with elemental sulfur in pyridine to lead to the corresponding 2-thio-1,3,2-oxathiaphospholane (**3**).[43] Intermediate **3** reacted with methanol in the presence of a strong base (DBU). Following deprotection (ammonium hydroxide solution), the resulting phosphorothioate was converted into its sodium salt G−P(O⁻)=S Na⁺ (Dowex Na⁺; 56% yield), and it is described below in more detail.

A round bottom flask (25 mL) was charged with acyl-protected 2′-deoxyguanosine **1** (0.190 g, 0.501 mmol), anhydrous pyridine (7 mL), and elemental sulfur (0.128 g, 0.501 mmol). 2-Chloro-1,3,2-oxathiaphospholane **2** (0.086 g, 0.60 mmol) was added dropwise with stirring. The reaction mixture was stirred at rt. (room temperature) for 12 h. The solvent was removed in vacuum, and the residue was triturated with acetonitrile (10 mL). Undissolved sulfur was filtered off, and the filtrate was concentrated in vacuum. The residue was dissolved in chloroform (2−3 mL). Silica gel column chromatography (2.5 × 18 cm, methanol in chloroform 0 → 5%) gave **3** as a white foam (0.156 g, 0.300 mmol; 60%). A round bottom flask (25 mL) was charged with **3** (156 mg, 0.300 mmol), anhydrous methanol (5 mL). DBU (55 μL, 0.36 mmol) was added, and the mixture was stirred for 6 h at rt. The solvent was removed by rotary evaporation, and the residue was dissolved in ammonium hydroxide solution (25%, 5 mL, removal of the protecting groups). The solvent was removed by rotary evaporation. Ion exchange column chromatography (DEAE-Sephadex A-25; eluent TEAB, 0 → 0.6 M, pH 7.5) gave phosphorothioate nucleoside as a triethylammonium salt G−P(O⁻)=S Et_3N^+. Subsequent ion

https://doi.org/10.1021/acs.jpcb.1c09068
J. Phys. Chem. B 2022, 126, 430−442

exchange chromatography (Dowex 50 WX4 Na^+) produced phosphorothioate nucleoside sodium salt G−P(O^-)=S Na^+, isolated as a white foam (0.063 g, 0.17 mmol; 56%). HRMS (ESI-TOF) $[M - H]^-$ calcd for $C_{11}H_{16}N_5O_6PS$ 376.0484, found 376.0486. NMR (D_2O, δ): ^1H 7.94 (d, J = 2.5 Hz, 1H, H-8), 6.14 (dt J = 6.8, 2.4 Hz, 1H, H-1′), 4.56 (ddd, J = 6.0, 3.1, 3.1 Hz, 1H, H-3′), 4.11−4.08 (m, 1H, H-4′), 3.97−3.88 (m, 2H, H-5′, H-5″), 3.36 (d, J = 12.7 Hz, 3H, CH_3), 2.71-2.62 (m, 1H, H-2″), 2.38 (ddd, J = 14.0, 6.4, 3.6 Hz, 1H, H-2′); $^{13}C\{1H\}$ 159.00, 153.87, 151.32, 137.51 and 137.43, 116.15, 85.53 (J = 5.5 Hz) and 85.46 (J = 5.5 Hz), 83.63 and 83.53, 71.37 and 71.27, 65.27 and 65.12, 52.77 (J = 6.0 Hz) and 52.76 (J = 6.4 Hz), 38.56 and 38.52; $^{31}P\{1H\}$ 57.46, 57.40. RP-HPLC: R_t = 15.91; 16.33 min.

3.2.2. Synthesis of the Phosphorothioate Model Compound, DMTP(O^-)=S Na^+. Dimethyl phosphorothioate sodium salt was prepared from diethyl phosphite in a manner analogous to the reported protocol, with a comparable yield of 94%. As a thionation system, elemental sulfur/pyridine/triethylamine was used, instead of benzoyl disulfide/dichloromethane/*N*,*N*-diisopropylethylamine.[44]

3.3. ESR Spectroscopic Studies. *3.3.1. Formation of −P−S∴Cl and [−P−S∴S−P−]$^-$ in the Homogeneous Glassy Solution of DMTP(O^-)=S (2 mg/mL).* The ESR spectrum shown in Figure 2A (400 G scan) has been obtained at 77 K

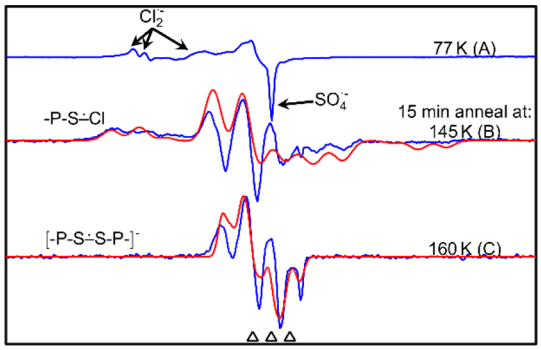

Figure 2. (A) ESR spectrum (blue) showing $SO_4^{\bullet-}$ and $Cl_2^{\bullet-}$ formation in γ-irradiated (absorbed dose = 1.4 kGy at 77 K) homogeneous glassy sample of DMTP(O^-)=S (2 mg/mL) in the presence of electron scavenger $K_2S_2O_8$ at native pD of 7.5 M LiCl/D_2O (ca. 5). (B) Spectrum of the sample in (A) after annealing at ca. 145 K for 15 min in the dark.(C) Further annealing at ca. 160 K for 15 min. Red spectra in (B) and (C) are the simulated ESR spectra. These are superimposed on the experimentally recorded spectra and are assigned to −P−S∴Cl and [−P−S∴S−P−]$^-$, respectively (for simulation parameters, see text). The experimental spectra shown in A, B, and C of this figure are also presented in Figure 3. All experimentally obtained spectra were recorded at 77 K. The three reference markers (open triangles) represent Fremy's salt resonance position separated from each other by 13.09 G with the central marker at g = 2.0056.

using a γ-irradiated homogeneous glassy (7.5 M LiCl/D_2O) sample of DMTP(O^-)=S (2 mg/mL). Following our previous studies, this spectrum shows the expected two low-field resonances from the dichloride anion radical, $Cl_2^{\bullet-}$, and a sharp singlet due to the sulfate anion radical, $SO_4^{\bullet-}$, at the center.[18,20,45,59]

$Cl_2^{\bullet-}$, the matrix radical, is formed due to scavenging of a radiation-produced hole by the glassy matrix (7.5 M LiCl) via the following reactions:[18,20,45]

$$h^+ + Cl^- \rightarrow Cl^{\bullet} \quad (1a)$$

$$Cl^- + Cl^{\bullet} \rightarrow Cl_2^{\bullet-} \quad (1b)$$

Scavenging of radiation-produced solvated electrons by $S_2O_8^{2-}$ leads to the formation of $SO_4^{\bullet-}$ (reaction 2).[18,20,45]

$$e_s^- + S_2O_8^{2-} \rightarrow SO_4^{2-} + SO_4^{\bullet-} \quad (2)$$

The glassy matrix (7.5 M LiCl) becomes gradually softened due to annealing (warming) at and above ca. 125 K; this facilitates migration of radicals. Thus, $SO_4^{\bullet-}$ can oxidize the matrix (Cl^-), thereby forming additional $Cl_2^{\bullet-}$ (reaction 3).[18,20,46,47]

$$SO_4^{\bullet-} + 2Cl^- \rightarrow SO_4^{2-} + Cl_2^{\bullet-} \quad (3)$$

As a result, the solute, DMTP(O^-)=S, reacts with the only radical species, $Cl_2^{\bullet-}$.[18,20,45]

We assign the spectrum (B, Figure 2) after annealing at ca. 145 K for 15 min to the $\sigma^2\sigma^{*1}$ adduct radical, −P−S∴Cl, as found in our earlier work on the formation of a $\sigma^2\sigma^{*1}$ adduct radical (−P−S∴Cl) via reaction of $Cl_2^{\bullet-}$ with DIP.[18] Here, −P−S∴Cl formation occurs via reaction of $Cl_2^{\bullet-}$ with DMTP(O^-)=S (reaction 4).

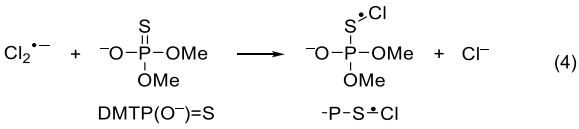

(4)

This spectrum has a central doublet (ca. 18 G) due to an isotropic α-P-coupling and a characteristic quartet owing to a single anisotropic Cl with an $A_{||}$ ^{35}Cl of ca. 63 G (see Table 1). Using these HFCCs, a simulated spectrum (red) has been generated, which shows a good match with experimental data. The HFCCs due to single anisotropic Cl, an isotropic α-P, and the anisotropic g-values of the −P−S∴Cl spectrum from DMTP(O^-)=S (this work) are compared with those reported for the −P−S∴Cl spectrum from DIP[18] (Table 1).

The ESR spectrum (C, Figure 2) obtained after subsequent annealing of the sample at ca. 160 K for 15 min in the dark is found to be different from that of the $\sigma^2\sigma^{*1}$ adduct radical, −P−S∴Cl (reaction 4, Figure 2 trace B). Based on our previous work on the formation of the $\sigma^2\sigma^{*1}$ adduct radical, [−P−S∴S−P−]$^-$, via the addition of −P−S∴Cl with the unreacted parent DIP;[18] the blue spectrum in Figure 2C has been assigned to the $\sigma^2\sigma^{*1}$ adduct radical, [−P−S∴S−P−]$^-$. It is the reaction of −P−S∴Cl with the unreacted parent DMTP(O^-)=S that leads to the formation of [−P−S∴S−P−]$^-$ (reaction 5).

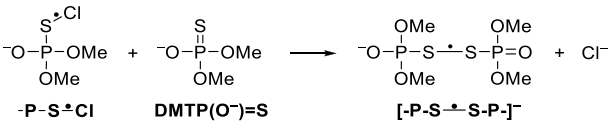

(5)

The spectrum (C) in Figure 2 shows two isotropic couplings assigned to two α-P. A simulation of this spectrum (red C, Figure 2) employing two isotropic α-P-atom couplings of ca. 10.0 G and ca. 12.5 G (see Table 1) along with a mixed Lorentzian/Gaussian (1/1) isotropic linewidth (5 G) and g-values (1.9997, 2.011, and 2.01585) shows a good match between the simulated (red) and experimentally obtained (blue) spectra.

In Figure 3, the experimentally obtained ESR spectra of DMTP(O^-)=S are compared with those reported from

https://doi.org/10.1021/acs.jpcb.1c09068
J. Phys. Chem. B 2022, 126, 430−442

Table 1. Experimental and B3LYP-PCM/6-31++G(d)-Calculated HFCCs in Gauss (G) and Experimental *g*-Values for −P−S∴Cl and [−P−S∴S−P−]$^-$ from DIP and DMTP(O$^-$)=S samples[a,b]

molecule	radical	nuclei	HFCC (G) exp	HFCC (G) theory	*g*-values
DMTP(O$^-$)=S	−P−S∴Cl[c]	^{35}Cl	ca. 63	1.24, 1.26, 63.29	2.0098, 2.00895, 2.0035
		^{37}Cl	ca. 52.5		
		P	ca. 18	−13.82, −13.11, −12.82	
	[−P−S∴S−P−]$^-$[d]	P1	ca. 10.0	−12.65, −12.06, −11.46	1.9997, 2.011, 2.01585
		P2	ca. 12.5	−10.08, −9.3, −8.31	
DIP[18] (see Figure 3)	−P−S∴Cl[c]	^{35}Cl	ca. 67	−1.84, −1.79, 70.87	2.014, 2.014, 2.0028
		^{37}Cl	ca. 55.8		
		P	ca. 23	−12.78, −12.26, −11.89	
	[−P−S∴S−P−]$^-$[e]	P1	6.0, 9.0, 7.0	−9.8, −9.19, −7.77	1.99939, 2.0046, 2.0270
		P2	16.0, 16.0, 17.0	−11.89, −11.56, −10.56	

[a]Experiment gives the magnitude but not the sign of the coupling. [b]The ^{35}Cl isotope has 75% abundance. [c]Lorentzian/Gaussian = 1 and linewidth = 10 G were used to obtain the simulated spectrum (red) in Figure 2B. [d]Lorentzian/Gaussian = 1 and linewidth = 5 G were used to obtain the simulated spectrum (red) in Figure 2C. [e]Lorentzian/Gaussian = 1 and linewidth = (3.5, 4.5, and 3.5) G were used to obtain the simulated spectrum.[18]

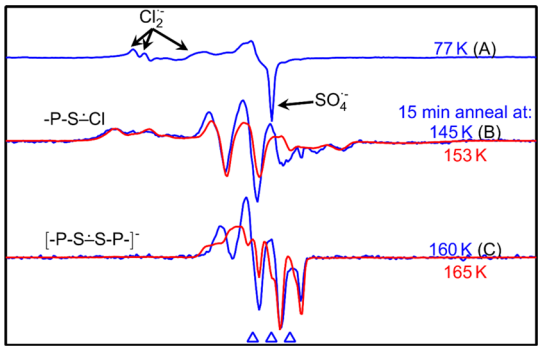

Figure 3. ESR spectra of a homogeneous glassy sample of DMTP(O$^-$)=S (2 mg/mL, blue) and DIP[18] (2 mg/mL, red) in the presence of electron scavenger $K_2S_2O_8$ at a native pD of 7.5 M LiCl/D_2O (ca. 5). (A) $SO_4^{\bullet-}$ and $Cl_2^{\bullet-}$ formation in *γ*-irradiated (1.4 kGy at 77 K). (B) Spectrum of the sample in (A) after annealing at ca. 145 K and ca. 153 K for 15 min in the dark. (C) Further annealing at ca. 155 K for 15 min and ca. 165 K for 20 min in the dark. All experimentally obtained spectra were recorded at 77 K. The three reference markers (open triangles) represent Fremy's salt resonance position separated from each other by 13.09 G with the central marker at *g* = 2.0056.

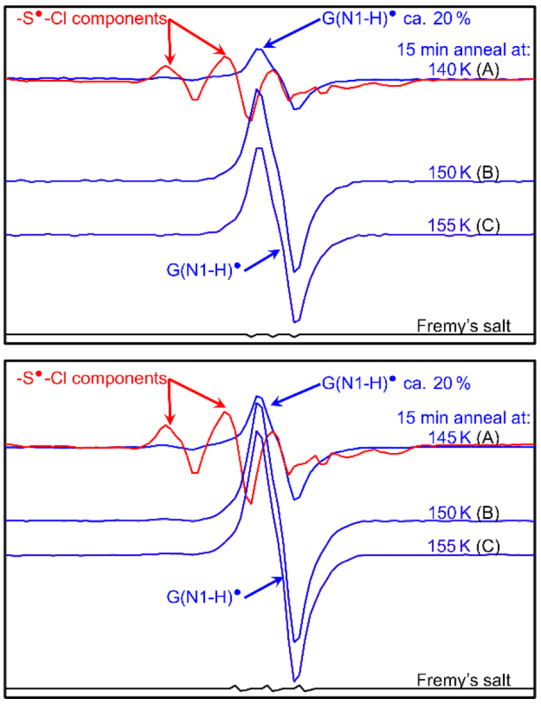

Figure 4. ESR spectra (250 G scan) of *γ*-irradiated (absorbed dose = 1.4 kGy at 77 K) homogeneous glassy samples of G−P(O$^-$)=S 2 mg/mL (A, Top panel) and 11 mg/mL (A, Top panel) in the presence of electron scavenger $K_2S_2O_8$ at a native pD of 7.5 M LiCl/D_2O (ca. 5). (A) Spectrum of the sample after annealing to ca. 140 K (top) and at ca. 145 K (bottom) in the dark for 15 min. The red spectrum in (A) in both panels is the spectrum B in Figure 2 assigned to −P−S∴Cl from DMTP(O$^-$)=S. (B) Spectra after annealing at ca. 150 K for 15 min in the dark in both panels. (C) Spectra after annealing at ca. 155 K for 15 min in the dark in both panels. All experimentally obtained spectra were recorded at 77 K. Spectra in panels B and C match with the reported spectrum of guanine cation radical (G$^{\bullet+}$) found in homogeneous glassy samples of dGuo or guanine containing DNA-oligonucleotides, respectively.[18,45−48]

DIP.[18] Comparison of HFCCs and *g*-values of the $\sigma^2\sigma^{*1}$ adduct radicals, −P−S∴Cl and [−P−S∴S−P−]$^-$, from DMTP(O$^-$)=S (this work) with the corresponding ones reported from DIP[18] (see Table 1) shows differences in the magnitude of the anisotropic Cl HFCCs and in the nature and extent of *α*-P HFCCs as well as in their *g*-values. It is apparent from Table 1 and Figure 3 that there is a significant difference in HFCCs and *g*-values are found to be pronounced for [−P−S∴S−P−]$^-$ from DMTP(O$^-$)=S and DIP. We attribute these differences to the differences in the inductive and hyperconjugation effects of the methyl and isopropyl groups.

3.3.2. Evidence of Backbone-to-Base Hole Transfer in the Samples of G−P(O$^-$)=S. Based on our previous studies on backbone-to-base hole transfer in an S-oligomers containing guanine,[18] ESR investigations were carried out employing matched samples of G−P(O$^-$)=S at two different concentrations 2 and 11 mg/mL to test for hole transfer from P−S∴Cl to G as well as [−P−S∴S−P−]$^-$ formation (Schemes 2 and 3). These results are shown in Figure 4. These samples were first *γ*-irradiated at 77 K and subsequently been annealed to ca. 140 K (Figure 4 top) and at ca. 145 K (Figure 4 bottom) for 15 min in the dark, and their ESR spectra are presented as spectra A in both panels of Figure 4. ESR spectra obtained

https://doi.org/10.1021/acs.jpcb.1c09068
J. Phys. Chem. B 2022, 126, 430−442

after subsequent annealing of these samples to ca. 150 K (B) and then at ca. 155 K (C) are presented in both panels of Figure 4. These spectra were recorded under the same conditions (constant gain and constant microwave power).

The −P−S∴Cl spectrum obtained from DMTP(O⁻)=S samples (spectra B of Figures 2 and 3) has been superimposed (A) in both panels of Figure 4. This superimposition shows that the spectra in both panels in Figure 4 have the line components due to the −P−S∴Cl (ca. 80%) and a singlet spectrum (ca. 20%) (reactions 6 and 7). ESR characteristics of the singlet (g value at the center, $g_\perp$, the total width, and the lineshape) match very well with the already published ESR spectrum of ($G^{\bullet+}$) from dGuo recorded under the same conditions [at 77 K at the native pD (ca. 5) in 7.5 M LiCl/D_2O].[45−48] So, the spectra shown in both panels in Figure 4A are composed of ca. 80% of the −P−S∴Cl spectrum from DMTP(O⁻)=S and ca. 20% of $G^{\bullet+}$ (reactions 6 and 7). Hence, the singlet found at the center of all spectra in Figure 4 is assigned to $G^{\bullet+}$ (hole). The spectra at ca. 155 K (Figure 4C) in both panels show primarily the spectra of $G^{\bullet+}$. Comparing the spectra in Figure 4C with those in Figures 2C and 3C, we conclude that the bimolecular formation of [−P−S∴S−P−]⁻ was not observed in G−P(O⁻)=S at high concentration.

$$Cl_2^{\bullet-} + G{-}P(O^-){=}S \xrightarrow{\text{ca.80\%, addition}} G{-}P(O^-){-}S{\therefore}Cl + Cl^- \quad (6)$$

$$Cl_2^{\bullet-} + G \xrightarrow{\text{ca.20\%, one-electron transfer}} G^{\bullet+} + 2Cl^- \quad (7)$$

$$G{-}P(O^-){-}S{\therefore}Cl \xrightarrow{\text{backbone-to-base hole transfer}} G^{\bullet+}{-}P(O^-){=}S + Cl^- \quad (8)$$

The spectra (B and C) in both panels of Figure 4 were recorded under the same conditions (constant gain and constant microwave power). These spectra establish that the line components of −P−S∴Cl progressively decrease (by a factor of ca. 4) upon annealing, while the singlet at the center due to $G^{\bullet+}$ increases by a factor of ca. 2. Thus, these results provide clear evidence for thermally activated hole transfer from −P−S∴Cl to the G moiety of G−P(O⁻)=S forming $G^{\bullet+}$ (reaction 8), confirming our previous work on S-oligomers (reaction 8).[18]

3.4. Pulse Radiolysis. Recent laser flash photolysis and time-dependent DFT calculations on phosphorothioates [O,O′-diethyl thiophosphate (DEP) and S-oligomers] in aqueous solutions at room temperature proposed the formation of −P−S∴Br and [−P−S∴S−P−]⁻.[49] However, our very recent work on phosphorodithioates combining synthesis, ESR in homogeneous glassy solutions at low temperature, and pulse radiolysis in aqueous solutions at room temperature showed that the $\sigma^2\sigma^{*1}$ adduct radical, [−P−2S∴2S−P−]⁻, was indeed detected by ESR only at low temperature and not by pulse radiolysis at room temperature.[20] This difference was attributed to the weak two-center three-electron bonding in [−P−2S∴2S−P−]⁻ that dissociated at room temperature. Therefore, we have carried out pulse radiolysis to verify the formation of $\sigma^2\sigma^{*1}$ adduct radicals, for example, −P−S∴Cl and [−P−S∴S−P−]⁻, in an aqueous solution to test the stability of both −P−S∴Cl and [−P−S∴S−P−]⁻ at room temperature, and the results of these investigations are presented below.

We performed the oxidation of DMTP(O⁻)=S by employing pulse radiolysis in aqueous solutions at room temperature with the aid of $Cl_2^{\bullet-}$, $^\bullet OH$, $SO_4^{\bullet-}$ and $N_3^\bullet$ radicals.

Radiolytically, the hydroxyl radicals ($^\bullet OH$) in N_2O-saturated aqueous solutions are produced according to reactions 9 and 10.[50−56]

$$H_2O \xrightarrow{\gamma} e_{aq}^-(2.8), H_3O^+, {}^\bullet H(0.6), {}^\bullet OH(2.8), H_2O_2\ (0.7) \quad (9)$$

$$e_{aq}^- + N_2O \rightarrow {}^\bullet OH + N_2 + OH^-(k_{10} = 9.1 \times 10^9\ M^{-1}\ s^{-1}) \quad (10)$$

In the presence of chloride anion (Cl^-), the $^\bullet OH$ are converted into $Cl_2^{\bullet-}$ (reactions 11−15).[20,50−56]

$$^\bullet OH + Cl^- \rightleftarrows ClOH^{\bullet-}(k_{11} = 4.3 \times 10^9\ M^{-1}\ s^{-1},\ k_{-11} = 6.1 \times 10^9\ s^{-1}) \quad (11)$$

$$ClOH^{\bullet-} + H^+ \rightleftarrows (HOClH)^\bullet\ (k_{12} = 3.0 \times 10^{10}\ M^{-1}\ s^{-1},\ k_{-12} = 1.0 \times 10^8\ s^{-1}) \quad (12)$$

$$(HOClH)^\bullet \rightleftarrows Cl^\bullet + H_2O\ (k_{13} = (5 \pm 2) \times 10^{14}\ s^{-1},\ k_{-13} = 2.5 \times 10^5\ M^{-1}\ s^{-1}) \quad (13)$$

$$Cl^\bullet + Cl^- \rightleftarrows Cl_2^{\bullet-}\ (k_{14} = (8.5 \pm 0.6) \times 10^9\ M^{-1}s^{-1},\ k_{-14} = (6.0 \pm 0.5) \times 10^4\ s^{-1}) \quad (14)$$

$$Cl_2^{\bullet-} + H_2O \rightleftarrows (HOClH)^\bullet + Cl^-\ (k_{15} = 1300\ M^{-1}s^{-1},\ k_{-15} = (8 \pm 2) \times 10^9\ M^{-1}\ s^{-1}) \quad (15)$$

In the presence of azide anion (N_3^-), the $^\bullet OH$ are converted into azide radicals ($N_3^\bullet$, reaction 16).[50,51,56]

$$^\bullet OH + N_3^- \rightarrow OH^- + N_3^\bullet(k_{16} = 1.2 \times 10^{10}\ M^{-1}\ s^{-1}) \quad (16)$$

Radiation chemical generation of $SO_4^{\bullet-}$ in aqueous solution involves the reaction of radiation-produced e_{aq}^- with persulfate anions ($S_2O_8^{2-}$) (reaction 17) in the presence of a high concentration of t-butanol as the scavenger of $^\bullet OH$.[20,50,57]

$$e_{aq}^- + S_2O_8^{2-} \rightarrow SO_4^{\bullet-} + SO_4^{2-}\ (k_{17} = 1.2 \times 10^{10}\ M^{-1}\ s^{-1}) \quad (17)$$

3.4.1. $Cl_2^{\bullet-}$-Mediated Oxidation of DMTP(O⁻)=S. To study the $Cl_2^{\bullet-}$-mediated reactions employing pulse radiolysis, N_2O-saturated aqueous solutions with low pH (pH = 2.8) having Cl^- concentration ([NaCl] = 1 mM) that is much higher than the substrate concentration (i.e., [DMTP(O⁻)=S] = 2.5×10^{-4} M) are used. These conditions ensure efficient $Cl_2^{\bullet-}$ formation (reactions 11−15).

3.4.1.1. Formation of the Thiyl Radical (−P−S$^\bullet$). Based on Hasegawa and Neta's work[58] on the formation of $Cl_2^{\bullet-}$ and its reaction with various compounds, we assign the absorption spectrum with a maximum at 345 nm[59] shown in Figure 5B to $Cl_2^{\bullet-}$ that is formed within 0.2 μs after the pulse (Figure 5A inset).

Figure 5B also presents another absorption spectrum with a maximum at 410 nm. This spectrum is assigned to the one-electron oxidized DMTP(O⁻)=S. Su and co-workers obtained a very similar spectrum by carrying out laser flash photolysis of

https://doi.org/10.1021/acs.jpcb.1c09068
J. Phys. Chem. B 2022, 126, 430−442

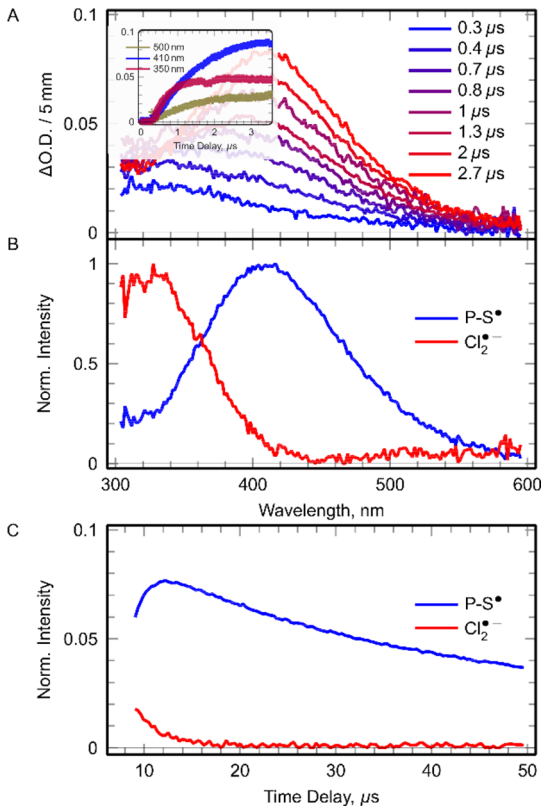

Figure 5. Pulse radiolysis of N_2O saturated solution at pH = 2.8 of DMTP(O^-)=S, 2.5×10^{-4} M in the presence of 1 mM NaCl. (A) Evolution of transient absorption spectra in time. Inset: Kinetics observed at three wavelengths. (B) Deconvoluted absorption spectra (C) and the kinetics of the two species $Cl_2^{\bullet-}$ and −P−S•. (B) and (C) were obtained from the analysis of the spectro-kinetic matrix data (see Figure S1).

DEP in the presence of $Na_2S_2O_8$ and LiCl[49] as well as of $Na_2S_2O_8$ and LiBr.[49] Based on the first radical chemical studies carried out on DIP and S-oligomers employing ESR spectroscopy at low temperature,[18] Su and co-workers assigned this spectrum to the $\sigma^2\sigma^{*1}$ adduct radicals, −P−S∴Cl (reactions 4 and 6, in the presence LiCl) and −P−S∴Br.[49] However, we assign the absorption spectrum in Figure 5B to the thiyl radical, −P−S• (reaction 18). Deconvolution of the spectrokinetic data (see Figure S1) presented in Figure 5B,C shows that the decay of $Cl_2^{\bullet-}$ formed after the pulse correlates with the build-up of −P−S• that absorbs at 410 nm, according to the following reaction 18.

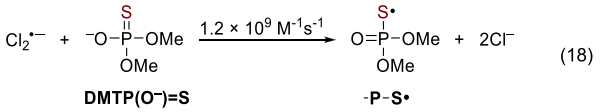

(18)

The −P−S• is formed via one-electron oxidation of DMTP(O^-)=S by $Cl_2^{\bullet-}$ (E° $Cl_2^{\bullet-}/2Cl^-$ = 2.1−2.3 V[52,60,61]), and the rate constant of this reaction at 298 K is measured as 1.2×10^9 M^{-1} s^{-1} (reaction 18). Thus, contrary to our ESR studies[18] (Figures 234, Table 1) and contrary to the proposed interpretation of the absorption spectrum in Figure 5A from laser flash photolysis in aqueous solution at room temperature,[49] our pulse radiolysis data convincingly show that the formation of −P−S∴Cl happens only at low temperature but not at room temperature owing to the weak bonding in the $\sigma^2\sigma^{*1}$ adduct.

3.4.1.2. Decay of −P−S•. -P-S• formed via reaction 18 disappears without forming the $\sigma^2\sigma^{*1}$ adduct radical, [−P−S∴S−P−]$^-$, unlike our ESR studies in homogeneous glassy solutions at low temperature[18] (Figures 2−4, Table 1) and unlike the laser flash photolysis in aqueous solution at room temperature. We conclude that the main reaction for −P−S• is the dimerization to form a stable diamagnetic molecule, [−P−S−S−P−] (reaction 19, see Section 2b for this assignment), absorbing either in UV or with a low extinction coefficient. Thus, it could not be detected at a longer wavelength than 300 nm.

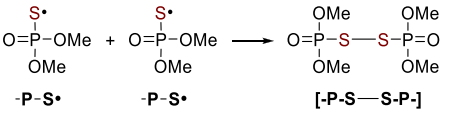

(19)

3.4.2. OH-Mediated Oxidation of DMTP(O^-)=S. 3.4.2.1. One-Electron Oxidation of DMTP(O^-)=S by •OH Causes the Thiyl Radical (−P−S•) Formation. To investigate the reaction of •OH with DMTP(O^-)=S by pulse radiolysis, we have used N_2O-saturated aqueous solution of 2.5×10^{-4} M DMTP(O^-)=S. Figure 6 presents the formation of an intense

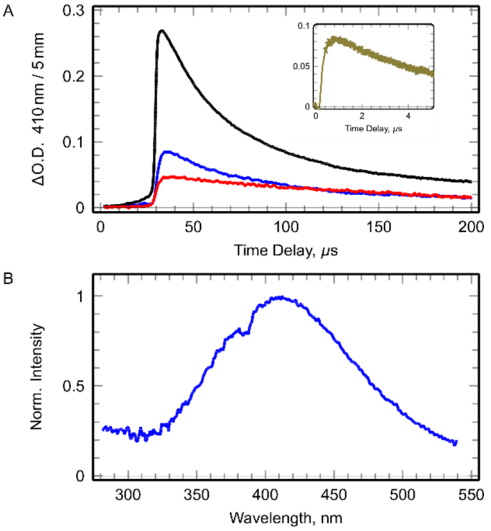

Figure 6. Pulse radiolysis of N_2O-saturated solution (pH = 7) of 2.5×10^{-3}(black) and 2.5×10^{-4} M DMTP(O^-)=S (blue and red) after the pulse at 90 Gy/pulse (black and blue) and 30 Gy/pulse (red). (A) Kinetics of formation and decay of the thiyl radical, P−S•, at different dose; inset: formation and decay of P−S• in the 5 μs range (90 Gy/pulse) and (B) deconvoluted absorption spectrum.

absorption band at 410 nm (B) and its decay followed up to 200 μs after the electron pulse (Figure 6A). The maximum absorption has been observed at around 1 μs; subsequently, this band decays without any change in its shape (Figure 6B).

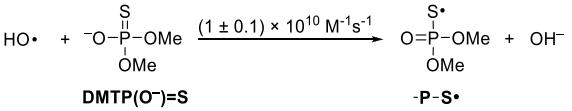

(20)

As the absorption spectrum (Figure 5B) of the radical formed via reaction of $Cl_2^{\bullet-}$ with DMTP(O^-)=S (reaction 18) matches well with the absorption spectrum of the radical (Figure 6A, black) produced due to reaction of •OH with DMTP(O^-)=S (reaction 20), we conclude that both reactions form the same radical species and it is not a $\sigma^2\sigma^{*1}$ adduct radical, for example, −P−S∴Cl or −P−S∴OH. We

https://doi.org/10.1021/acs.jpcb.1c09068
J. Phys. Chem. B 2022, 126, 430−442

assign this radical species as the thiyl radical, −P−S$^{\bullet}$ (reactions 18 and 20) and is formed via one-electron oxidation of DMTP(O$^-$)=S by either $Cl_2^{\bullet-}$ (reaction 18) or by $^{\bullet}$OH (E° $^{\bullet}$OH, H$^+$/H_2O = 2.73 V)[50,61] midpoint potential (E_7 $^{\bullet}$OH, H$^+$/H_2O = 2.3 V,[50,62,63] reaction 20).

The rate constant of reaction 20 was determined as (1 ± 0.1) 10^{10} M^{-1} s^{-1}. Thus, the rate of reaction 20 is almost one order of magnitude higher than that of reaction 18.

3.4.2.2. Decay of −P−S$^{\bullet}$. −P−S$^{\bullet}$ decays with a rate constant of about 3.5 × 10^7 M^{-1} s^{-1} (Figure 6A). The product of the decay does not absorb in the region 300−600 nm. The decay follows predominantly a second-order kinetics (Figure S2). Consequently, −P−S$^{\bullet}$ undergoes dimerization to form a stable diamagnetic molecule, [−P−S−S−P−] (reaction 19).

3.4.3. Reaction of $SO_4^{\bullet-}$ and $N_3^{\bullet}$ with DMTP(O$^-$)=S. The standard reduction potential of $SO_4^{\bullet-}$ was reported as ($SO_4^{\bullet-}$/SO_4^{2-}) = 2.44 V.[50,61] $SO_4^{\bullet-}$ was generated via reaction 17 in the presence of $^{\bullet}$OH scavenger, that is, *t*-butanol.[20,50] $SO_4^{\bullet-}$ oxidizes DMTP(O$^-$)=S forming −P−S$^{\bullet}$ (reaction 21 and Figure S3), and the rate constant of this reaction has been measured as = 1 × 10^9 M^{-1} s^{-1}.

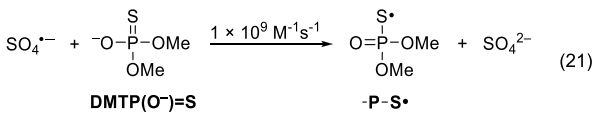

(21)

However, pulse radiolysis measurements showed that $N_3^{\bullet}$ does not oxidize DMTP(O$^-$)=S, thereby establishing that the redox potential of −P−S$^{\bullet}$ is higher than that of $N_3^{\bullet}$ (E° ($N_3^{\bullet}$/N_3^-) = 1.33 V[50,51,55,56,61]).

3.4.4. Oxidation of Guo by −P−S$^{\bullet}$ from DMTP(O$^-$)=S. As described in Sections 123 above, DMTP(O$^-$)=S is oxidized by $Cl_2^{\bullet-}$, $^{\bullet}$OH, and $SO_4^{\bullet-}$ but not by $N_3^{\bullet}$. Based on these results, it is expected that the reduction potential of −P−S$^{\bullet}$ from DMTP(O$^-$)=S would be higher than either E° (G$^{\bullet+}$/G) = 1.49 V)[45,50,62,64,65] or E_7 (G(N1−H)$^{\bullet}$)/H$^+$, G) = 1.29 V.[45,50,62,64,65] In addition, using the DFT/ωB97xD-PCM/6-31++G** method, the calculated adiabatic ionization energy (AIE) values (in eV) for the guanine (G)-containing phosphorothioate (G-P(O$^-$)=S, 5.77 eV), phosphate (O4P-G, 5.76 V), and the abasic phosphorothioate (O_3PSEt_2, 5.85 eV) (see Supporting Information for their structures) showed that the phosphorothioate and the phosphate with G base have very similar AIEs with spin on the G base.[20]

On the other hand, the calculated AIE value of the abasic phosphorothioate is observed to be higher than that of the G−P(O$^-$)=S and the spin on the S-atom; hence, it is expected that in G−P(O$^-$)=S, the one-electron oxidized phosphorothioate moiety would oxidize the G base (i.e., backbone-to-base hole transfer process),[20] forming G$^{\bullet+}$ which would undergo subsequent reactions.[5−7,23,28−31,50,64]

To test this hypothesis, we have performed pulse radiolysis of the Ar-saturated solution (pH = 7) containing 5 × 10^{-5} M Guo, 5 × 10^{-4} M DMTP(O$^-$)=S, 0.2 M *t*-butanol as the $^{\bullet}$OH scavenger,[20] and 2 × 10^{-3} M $S_2O_8^{2-}$ as a solvated electron scavenger (reaction 17).

The absorption spectrum recorded at 40 μs after the pulse confirms the formation of −P−S$^{\bullet}$ from DMTP(O$^-$)=S absorbing at 410 nm (see Figure 7) via one-electron oxidation by $SO_4^{\bullet-}$ (reactions 17 and 21). Subsequently, the absorption spectrum recorded at 100 μs after the pulse confirms the formation of a guanyl radical with a prominent 300 nm band and a shoulder at 350 nm. ESR, pulse radiolysis, and flash photolysis have established that deprotonation of G$^{\bullet+}$ in nucleosides in single stranded (ss) oligomers and in the intrabase pair proton transfer process in double-stranded DNA-oligomers happens from the N1-site of the guanine base.[5,6,45−47,50,64,66−73] Pulse radiolysis and flash photolysis have established that the deprotonation of G$^{\bullet+}$ from N1 happens in the sub-μs region[67−71] and with the rate constant values as 1.8 × 10^7 s^{-1} (pulse radiolysis)[69,71] and 1.5 × 10^7 s^{-1} (flash photolysis).[70] In comparison of this spectrum with the reported G(N1-H)$^{\bullet}$ spectrum in the literature,[64,66−73] we attribute a significant part of the absorption spectrum recorded at 100 μs after the pulse to G(N1-H)$^{\bullet}$.

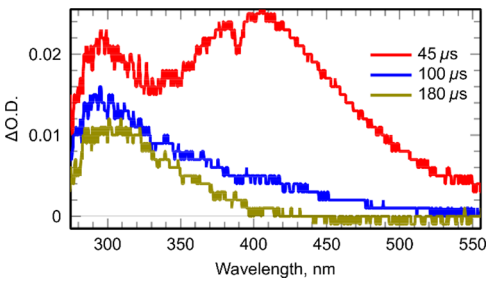

Figure 7. Absorption spectra recorded at different time delays employing pulse radiolysis of the Ar-saturated solution containing 5 × 10^{-5} M Guo, 5 × 10^{-4} M DMTP(O$^-$)=S, 0.2 M *t*-butanol, and 2 × 10^{-3} M $S_2O_8^{2-}$.

The decay of −P−S$^{\bullet}$ from DMTP(O$^-$)=S correlates with the formation of the guanyl radical, indicating that formation of the guanyl radical occurs via the intermolecular oxidation process, that is, −P−S$^{\bullet}$-mediated oxidation of Guo (reaction 22). It is interesting to note that the decay of −P−S$^{\bullet}$ from DMTP(O$^-$)=S has been observed to be faster upon increasing the concentration of Guo (see Figure S4).

Furthermore, at a longer time (180 μs) after the pulse, only the 300 nm band is observed, and the other two bands are not observed. This spectrum matches well with the reported spectrum $^{\bullet}$GOH (reaction 23).[73] It is well-established that $^{\bullet}$GOH formation occurs via nucleophilic attack of water at C-8 of the guanine cation radical (G$^{\bullet+}$) followed by deprotonation.[73−75] On this basis, we assign the absorption spectrum recorded at 100 μs after the pulse due to both G(N1-H)$^{\bullet}$ and $^{\bullet}$GOH. The estimated value of the rate constant for reaction 23 is 8 × 10^3 s^{-1}.

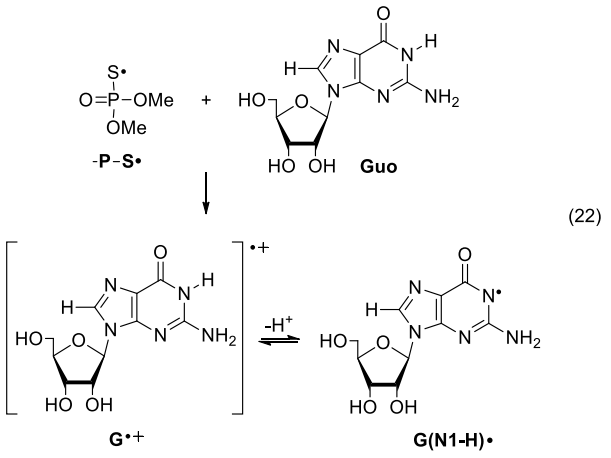

(22)

https://doi.org/10.1021/acs.jpcb.1c09068
J. Phys. Chem. B 2022, 126, 430−442

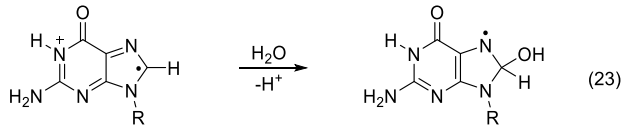

(23)

$G^{\bullet+}$ from Guo

3.4.5. Oxidation of the Guanine Base by −P−S• in G−P(O⁻)═S. Based on our observation that −P−S• can oxidize the guanine base in Guo (Section 4, above), we have carried out pulse radiolysis of Ar-saturated aqueous solution of 1.25×10^{-4} M G-P(O⁻)═S in the presence of 2×10^{-3} M $S_2O_8^{2-}$ as the radiation-produced electron scavenger (reaction 17) and 0.2 M *t*-butanol[20] (Figure 8).

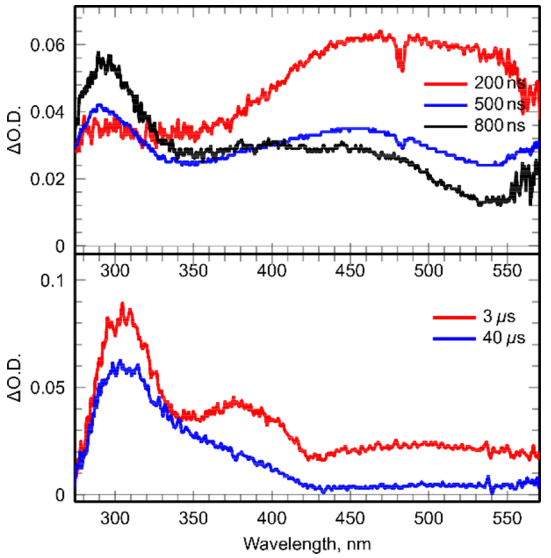

Figure 8. Absorption spectra (top and bottom) obtained by employing pulse radiolysis of Ar-saturated solution (pH = 7) of 1.25×10^{-3} M G-P(O⁻)═S in the presence of 2×10^{-3} M $S_2O_8^{2-}$, 0.2 M *t*-butanol at various time delays.

The pulse radiolysis has been performed at different timescales, and a few selected absorption spectra have been reported at 200 ns, 500 ns, 800 ns (top), 3, and 40 μs after the pulse, as shown in Figure 8. At 200 ns, the absorption band of the radical $SO_4^{\bullet-}$ with a contribution from the fully solvated electron (aqueous electron, e_{aq}^-) is observed. At 800 ns, the shape of the absorption band is broader in the visible region. At these timescales, we do not observe the characteristic absorption (410 nm) of −P−S•.

The absorption spectrum recorded at 2 μs after the pulse shows three well-defined bands at 480, 390, and 300 nm. This spectrum matches well with the reported spectrum of the conjugate base (N1-deprotonated form) of $G^{\bullet+}$, that is, G(N1-H)• in the literature.[20,47,50,63,64,66−73] Based on these results and on the results shown in Figure 7, we propose that the lifetime of the −P−S• produced via oxidation of G-P(O⁻)═S by $SO_4^{\bullet-}$ is very short in the range of ps (reaction 24). In fact, these data suggest that the intramolecular electron transfer is quite facile as if $G^{\bullet+}$ in G−P(O⁻)═S is produced via direct G base oxidation by $SO_4^{\bullet-}$.

Therefore, we assign the spectrum at 3 μs to G(N1-H)• from G−P(O⁻)═S. This result is clear evidence of intramolecular oxidation of the guanine base of G−P(O⁻)═S forming $G^{\bullet+}$ followed by its deprotonation. At a longer timescale, 40 μs after the pulse, the bands at 480 and 390 nm disappear; a new species is formed that absorbs at 300 nm with a shoulder around 370 nm, just similar to our observation in Figure 7. This spectrum matches well with the reported spectrum of •GOH (reaction 23).[73]

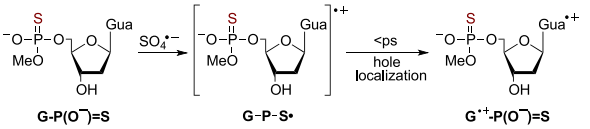

(24)

3.5. Theoretical Studies. Theoretical calculations were performed to elucidate the mechanisms of radical formation and their characterization as proposed by ESR investigations and pulse radiolysis. Using B3LYP-PCM/6-31++G(d) methodology, we calculated the spin density distributions, HFCC values, and thermochemical quantities such as free energy (G), enthalpy (H), and entropy (S) for reactions 4, 5, and 18 to explain the formation and stability of −P−S∴Cl and [−P−S∴S−P−]⁻ adducts at 298 K. Because the radicals that appear in reactions 4, 5, and 18 are localized cation radical systems, the use of B3LYP is quite appropriate,[18,47,66] as there is no issue with the well-known charge delocalization issues in these systems.

3.5.1. HFCCs. The B3LYP-PCM/6-31++G(d)-calculated HFCCs of −P−S∴Cl and [−P−S∴S−P−]⁻ along with their experimental values are presented in Table 1. For −P−S∴Cl adduct, ESR estimated couplings of ^{35}Cl and P are ca. 63 and 18 G, respectively. The calculated total HFCCs ($A_{iso} + A_{aniso}$) of ^{35}Cl are 1.24, 1.26, and 63.29 G, respectively (see Table 1 and Table S1). The total calculated α-P HFCCs are −13.82, −13.11, and −12.82 G, respectively (see Table 1 and Table S1). Following our previous studies on DIP, S-oligomers, and phosphorodithioates,[18,20] we find that a good match of ^{35}Cl with the experiment is evident, but the calculated HFCC of P is ca. 4 G less than the experimental value. For the [−P−S∴S−P−]⁻ adduct, the experimentally obtained α-P HFCCs are ca. 10 G and ca. 12.5 G, respectively. The corresponding calculated total HFCCs due to each α-P are −10.08, −9.3, and −8.31 G and −12.65, −12.07, and −11.46 G, which are in good agreement with the experimentally obtained HFCCs.

3.5.2. Relative Stability of Adducts with Temperature. We have theoretically tested the hypothesis that at low temperature (77 K), ESR predicts the −P−S∴Cl adduct radical formation. However, pulse radiolysis carried out at room temperature confirms the formation of −P−S•. To aid our understanding of temperature-dependent −P−S∴Cl adduct stability, we calculated the free energy (G), enthalpy (H), and entropy (S) of −P−S∴Cl, Cl⁻, and −P−S• at 298 K and calculated the dissociation energy for reaction (−P−S∴Cl → −P−S• + Cl⁻) (see Table S2). The calculated dissociation free energy (ΔG) is 0.4 kcal/mol, which evidences that −P−S∴Cl adduct is unbound (unstable) at room temperature and unequivocally supports the pulse radiolysis experiment. To gain insights into the stability at low temperature, we approximate the dissociation free energy at 0 K (neglecting the entropy contribution) to be 7.5 kcal/mol, which supports the presence of the −P−S∴Cl adduct at low temperature as proposed by ESR at 77 K. Similarly, the [−P−S∴S−P−]⁻ adduct is weakly stable at room temperature by 2.5 kcal/mol, while it is stabilized at 0 K by ca. 12 kcal/mol (see Table S2). Therefore, the combination of experimental and theoretical results reported in this work, along with our previous work on phosphorodithioates,[20] establishes that the $\sigma^2\sigma^{*1}$ adduct radicals −P−S∴Cl, [−P−S∴S−P−]⁻, and [−P−2S∴2S−

https://doi.org/10.1021/acs.jpcb.1c09068
J. Phys. Chem. B 2022, 126, 430−442

P−]$^-$ are stable at low temperature but not at room temperature.

4. CONCLUSIONS

This work has led to the following salient findings that include answers to the questions posed in the introduction of our work:

4.1. Synthesis of G−P(O$^-$)=S Na$^+$ and DMTP(O$^-$)=S Na$^+$. The syntheses of the 5′-phosphorothioate nucleoside, G−P(O$^-$)=S Na$^+$, and the modified protocol for the synthesis of DMTP(O$^-$)=S Na$^+$, both model compounds, are reported.

4.2. P−S∴Cl and [−P−S∴S−P−]$^-$ are Formed Only at Low Temperature. Similar to our previous work on phosphorothioates[18] and phosphorodithioates,[20] P−S∴Cl formation in DMTP(O$^-$)=S and G−P(O$^-$)=S and [−P−S∴S−P−]$^-$ production in DMTP(O$^-$)=S are observed employing ESR. However, pulse radiolysis show that both DMTP(O$^-$)=S and G−P(O$^-$)=S, via one-electron oxidation, form the thiyl radical (−P−S$^\bullet$), which did not lead to [−P−S∴S−P−]$^-$ formation. This work thus questions the laser flash photolysis report on P−S∴Cl formation in the aqueous solution of phosphorothioate at ambient temperature.[49] In addition, DFT calculations show that the bond enthalpy of −P−S∴Cl and [−P−S∴S−P−]$^-$ are 7.5 and 11.7 kcal/mol, respectively, which explains their stability at low temperatures. On the other hand, only −P−S$^\bullet$ formation was observed by pulse radiolysis measurements carried out at ambient temperatures due to the fact that the entropy of dissociation drives the equilibrium to the separate species (−P−S$^\bullet$).

4.3. The inductive Effect and Hyperconjugation Affect the ESR Parameters of −P−S∴Cl and [−P−S∴S−P−]$^-$. The differences observed in the HFCC values and *g*-values of −P−S∴Cl and [−P−S∴S−P−]$^-$ in DMTP(O$^-$)=S vs DIP are due to the inductive effects and in the hyperconjugation of isopropyl vs methyl groups.

4.4. The Backbone-To-Base Hole Transfer Process is Unimolecular and Facile and Occurs Via Hopping. According to the previous work from our laboratory on S-oligomers[18] and ESR studies employing samples having different concentrations (3 and 11 mg/mL) of the nucleotide, G−P(O$^-$)=S, P−S∴Cl oxidizes the G base (backbone-to-base hole transfer) in G−P(O$^-$)=S unimolecularly via thermally activated hopping.

The DFT calculations on AIE using the DFT/ωB97XDPCM/6-31++G** method predicted the oxidation of the G base by one-electron-oxidized phosphate and phosphorothioate[20] [see Section 4.4]. Pulse radiolysis validated this theoretical prediction and showed that the timescale of the backbone-to-base hole transfer process in G−P(O$^-$)=S is in the sub-picosecond range in aqueous solution at room temperature and the results are obtained by theoretical simulations.[20]

Our previous studies[17−22] proposed that successful formation of a sugar radical (e.g., C5′$^\bullet$) should occur via a very rapid (<10^{-12} s) deprotonation from the directly ionized sugar-phosphate backbone, even though longer-lived holes and electrons are successfully scavenged (Scheme 1). The rate of this deprotonation must be faster than that of energetically downhill transfer of the hole (unpaired spin) from the ionized sugar-phosphate backbone to the DNA base (backbone-to-base) hole transfer, which is in the sub-picosecond range (Scheme 1).

4.5. The Number of Sulfur Substitution in the Phosphate Group Controls the Directionality of the Hole Transfer Process between the Base and Backbone. Combining the results of G−P(O$^-$)=S with our previous studies on phosphorothioate[18] and on phosphorodithioate,[20] we have observed that hole transfer occurs from the backbone (P−(O$^-$)=S) to base in phosphorothioate-incorporated DNA and from the base to backbone (P−(S$^-$)=S) in phosphorodithioate-incorporated DNA. Thus, the directionality of transfer of the hole and its localization between the base and backbone is crucially controlled by the number of sulfur substitution in the phosphate group.

4.6. Being the First to Report the Rate of Hydration of the Guanyl Radical in the Phosphorothioate Monomer. This work reports the rate of hydration of the guanyl radical in the phosphorothioate monomer, G−P(O$^-$)=S, as 8×10^3 s^{-1}. This rate is expected, as the corresponding rate of hydration of one-electron-oxidized guanine in ds oligomers with the sugar-phosphate backbone and in highly polymerized calf thymus DNA has been reported to be much lower by one to two orders of magnitude;[73] this difference in the rate of hydration of the guanyl radical between the monomer and oligomers including calf thymus DNA is attributed to the difference in properties such as base stacking and water access and mobility between the monomer and the polymer.[50,76,77]

4.7. Biological Implication of these Results. Owing to the facile backbone-to-base hole transfer process in one-electron-oxidized phosphorothioate, the backbone would be protected more than the base as evidenced by $^\bullet$GOH formation (reaction 23). On the other hand, the base moieties in one-electron-oxidized phosphorodithioate would be protected more than the backbone due to the facile base-to-backbone hole transfer process.[20] Consequently, both phosphorothioate and phosphorodithoates can be predicted to augment radiation damage to cells, while phosphorodithoate would be more effective in causing radiation-induced cell death due to the backbone damage and to the S−S linkage formation between DNA and proteins[20] apart from affecting the repair processes via alteration of gene expression. These predictions need to be validated. We note here that phosphorothioate-mediated augmentation of radiation damage to cells has already been reported and has been proposed to improve the radiotherapeutic efficacy of liver cancer.[78]

■ ASSOCIATED CONTENT

Supporting Information

The Supporting Information is available free of charge at https://pubs.acs.org/doi/10.1021/acs.jpcb.1c09068.

Synthetic experimental section additional information, ^{1}H, ^{13}C, and ^{31}P NMR spectrum of G−P(O$^-$)=S Na$^+$, HPLC profile and HRMS spectrum of G−P(O$^-$)=S Na$^+$, ^{1}H, ^{13}C, and ^{31}P NMR spectrum of DMTP(O$^-$)=S Na$^+$, compounds used, ESR and theoretical methods, additional data of pulse radiolysis, and optimized geometries and thermochemical calculations (PDF)

■ AUTHOR INFORMATION

Corresponding Authors

Roman Dembinski − *Department of Chemistry, Oakland University, Rochester, Michigan 48309-4479, United States; Centre of Molecular and Macromolecular Studies, Polish*

https://doi.org/10.1021/acs.jpcb.1c09068
J. Phys. Chem. B 2022, 126, 430−442

Academy of Sciences, Łódź 90-363, Poland;
Phone: 0012483702248; Email: dembinsk@oakland.edu
Mehran Mostafavi − *Institut de Chimie Physique, UMR 8000 CNRS/Université Paris-Saclay, Orsay 91405 Cedex, France*; orcid.org/0000-0002-4510-8272;
Email: mehran.mostafavi@universite-paris-saclay.fr
Amitava Adhikary − *Department of Chemistry, Oakland University, Rochester, Michigan 48309-4479, United States*; orcid.org/0000-0001-9024-9579;
Phone: 0012483702094; Email: adhikary@oakland.edu;
Fax: 0012483702321

Authors

Sergey A. Denisov − *Institut de Chimie Physique, UMR 8000 CNRS/Université Paris-Saclay, Orsay 91405 Cedex, France*; orcid.org/0000-0001-7881-1979
Samuel Ward − *Department of Chemistry, Oakland University, Rochester, Michigan 48309-4479, United States*
Viacheslav Shcherbakov − *Institut de Chimie Physique, UMR 8000 CNRS/Université Paris-Saclay, Orsay 91405 Cedex, France*
Alexander D. Stark − *Department of Chemistry, Oakland University, Rochester, Michigan 48309-4479, United States*
Renata Kaczmarek − *Centre of Molecular and Macromolecular Studies, Polish Academy of Sciences, Łódź 90-363, Poland*
Ewa Radzikowska-Cieciura − *Centre of Molecular and Macromolecular Studies, Polish Academy of Sciences, Łódź 90-363, Poland*
Dipra Debnath − *Department of Chemistry, Oakland University, Rochester, Michigan 48309-4479, United States*
Taisiya Jacobs − *Department of Chemistry, Oakland University, Rochester, Michigan 48309-4479, United States*
Anil Kumar − *Department of Chemistry, Oakland University, Rochester, Michigan 48309-4479, United States*; orcid.org/0000-0002-9979-7798
Michael D. Sevilla − *Department of Chemistry, Oakland University, Rochester, Michigan 48309-4479, United States*; orcid.org/0000-0001-8799-5458
Pascal Pernot − *Institut de Chimie Physique, UMR 8000 CNRS/Université Paris-Saclay, Orsay 91405 Cedex, France*; orcid.org/0000-0001-8586-6222

Complete contact information is available at: https://pubs.acs.org/10.1021/acs.jpcb.1c09068

Notes

The authors declare no competing financial interest.

■ ACKNOWLEDGMENTS

A.A., A.K., and M.D.S. thank NIH NCI (Grant R01CA045424), A.A., M.D.S., and R.D. thank Research Excellence Fund (REF), and Center for Biomedical Research for support. R.K., E.R.-C., and R.D. thank NIH NCI (CA111329) and Statutory Funds of CMMS PAS for support. The authors are also thankful to Dr. Hiroyuki Hayakawa (Yamasa Corporation, Biochemicals Division) for a generous supply of nucleosides. The National Science Foundation (NSF) instrumentation awards (CHE-1920110, CHE-0722547, and CHE-0821487) are also acknowledged.

■ REFERENCES

(1) Becker, D.; Adhikary, A.; Sevilla, M. D. The Role of Charge and Spin Migration in DNA Radiation Damage. In *Charge Migration in DNA*, Ed. Chakraborty, T.; Springer-Verlag: Berlin, Heidelberg, 2007, 139−175.
(2) de La Lande, A.; Denisov, S.; Mostafavi, M. The mystery of sub-picosecond charge transfer following irradiation of hydrated uridine monophosphate. *Phys. Chem. Chem. Phys.* **2021**, *23*, 21148−21162.
(3) Kumar, A.; Sevilla, M. D. Proton Coupled Electron Transfer in DNA on Formation of Radiation Produced Ion Radicals. *Chem. Rev.* **2010**, *110*, 7002−7023.
(4) Kumar, A.; Sevilla, M. D. Theoretical Modeling of Radiation Induced DNA Damage. In *"Radicals and Radical Reactivity in Nucleic Acid Chemistry"*. Ed. Greenberg, M. M.; John Wiley and Sons, Inc.: New York, 2009, 1−40.
(5) Adhikary, A.; Becker, D.; Sevilla, M. D. Electron spin resonance of radicals in irradiated DNA. In *Applications of EPR in radiation research*, Eds. Lund, A., Shiotani, M.; Springer-Verlag: Berlin, Heidelberg, 2014, 299−352.
(6) Becker, D.; Kumar, A.; Adhikary, A.; Sevilla, M. D. Chapter 31. Gamma- and Ion-beam DNA Radiation Damage: Theory and Experiment. In *DNA Damage, DNA Repair and Disease*, *2*, Eds. Dizdaroglu, M., Llyod, R. S.; Royal Society of Chemistry (RSC): London, UK, 2020, 426−457.
(7) Bernhard, W. A. In *'Radical and Radical Ion Reactivity in Nucleic Acid Chemistry'*, Ed. Greenberg, M. M.; John Wiley & Sons, Inc.: New Jersey, 2009, 41−68.
(8) Close, D. M. In *Radiation-induced Molecular Phenomena in Nucleic Acids: A Comprehensive Theoretical and Experimental Analysis'*, Eds. Shukla, M. K., Leszczynski, J.; Springer-Verlag: Berlin, Heidelberg, New York, 2008, 493−529.
(9) Long Range Transfer in DNA II', ed. Shuster, G. B. *Topics in Current Chemistry*; Springer-Verlag, Berlin: Heidelberg, New York, 2004, *237*, 103−128.
(10) von Sonntag, C. In *Recent Trends in Radiation Chemistry*, Eds. Rao, B. S. M., Wishart, J.; World Scientific Publishing Co.: Singapore, New Jersey, London, 2010, 543−562.
(11) Genereux, J. C.; Barton, J. K. Mechanisms for DNA Charge Transport. *Chem. Rev.* **2010**, *110*, 1642−1662.
(12) Kanvah, S.; Joseph, J.; Schuster, G. B.; Barnett, R. N.; Cleveland, C. L.; Landman, U. Oxidation of DNA: damage to nucleobases. *Acc. Chem. Res.* **2010**, *43*, 280−287.
(13) Wagenknecht, H.-A. (eds.) *Charge Transfer in DNA: From Mechanism to Application*; Wiley-VCH Verlag GmbH & Co. KGaA: Weiheim, 2005, 1 −76.
(14) Frankenberg, D.; Frankenberg-Schwager, M.; Blöcher, D.; Harbich, R.; Blocher, D. Evidence for DNA double-strand breaks as the critical lesions in yeast cells irradiated with sparsely or densely ionizing radiation under oxic or anoxic conditions. *Radiat. Res.* **1981**, *88*, 524−532.
(15) Van Gent, D. C.; Hoeijmakers, J. H. J.; Kanaar, R. Chromosomal stability and the DNA double-stranded break connection. *Nat. Rev. Genet.* **2001**, *2*, 196−206.
(16) Ward, J. F. Complexity of Damage Produced by Ionizing Radiation. *Cold Spring Harb. Symp. Quant. Biol.* **2000**, *65*, 377−382.
(17) Adhikary, A.; Becker, D.; Palmer, B. J.; Heizer, A. N.; Sevilla, M. D. Direct formation of the C5'-radical in the sugar-phosphate backbone of DNA by high-energy radiation. *J. Phys. Chem. B* **2012**, *116*, 5900−5906.
(18) Adhikary, A.; Kumar, A.; Palmer, B. J.; Todd, A. D.; Sevilla, M. D. Formation of S-Cl phosphorothioate adduct radicals in dsDNA S-oligomers: Hole transfer to guanine vs disulfide anion radical formation. *J. Am. Chem. Soc.* **2013**, *135*, 12827−12838.
(19) Ma, J.; Marignier, J.-L.; Pernot, P.; Houée-Levin, C.; Kumar, A.; Sevilla, M. D.; Adhikary, A.; Mostafavi, M. Direct Observation of the Oxidation of DNA Bases by Phosphate Radical Formed Under Radiation: A Model of Backbone-to-base Hole Transfer. *Phys. Chem. Chem. Phys.* **2018**, *20*, 14927−14937.
(20) Kaczmarek, R.; Ward, S.; Debnath, D.; Jacobs, T.; Stark, A. D.; Korczyński, D.; Kumar, A.; Sevilla, M. D.; Denisov, S. A.; Shcherbakov, V.; Pernot, P.; Mostafavi, M.; Dembinski, R.; Adhikary, A. One Way Traffic: Base-to-backbone Hole Transfer in

Nucleoside Phosphorodithioates. *Chem. – Eur. J.* **2020**, *26*, 9495–9505.
(21) Ma, J.; Denisov, S. A.; Adhikary, A.; Mostafavi, M. Ultrafast Processes Occurring in Radiolysis of Highly Concentrated Solutions of Nucleosides/Tides. *Int. J. Mol. Sci.* **2019**, *20*, 4963.
(22) Ma, J.; Denisov, S. A.; Marignier, J.-L.; Pernot, P.; Adhikary, A.; Seki, S.; Mostafavi, M. Ultrafast electron attachment and hole transfer following ionizing radiation of aqueous uridine monophosphate. *J. Phys. Chem. Lett.* **2018**, *9*, 5105–5109.
(23) Sharma, K. K. K.; Tyagi, R.; Purkayastha, S.; Bernhard, W. A. One-electron oxidation of DNA by ionizing radiation: competition between base-to-base hole-transfer and hole-trapping. *J. Phys. Chem. B* **2010**, *114*, 7672–7680.
(24) Close, D. M. Where are the sugar radicals in irradiated DNA? *Radiat. Res.* **1997**, *147*, 663–673.
(25) Adhikary, A.; Malkhasian, A. Y.; Collins, S.; Koppen, J.; Becker, D.; Sevilla, M. D. UVA-visible photo-excitation of guanine radical cations produces sugar radicals in DNA and model structures. *Nucleic Acids Res.* **2005**, *33*, 5553–5564.
(26) Adhikary, A.; Becker, D.; Collins, S.; Koppen, J.; Sevilla, M. D. C5′- and C3′- sugar radicals produced via photo-excitation of one-electron oxidized adenine in 2′-deoxyadenosine and its derivatives. *Nucleic Acids Res.* **2006**, *34*, 1501–1511.
(27) Adhikary, A.; Kumar, A.; Sevilla, M. D. Photo-induced hole transfer from base to sugar in DNA: Relationship to primary radiation damage. *Radiat. Res.* **2006**, *165*, 479–484.
(28) Jaruga, P.; Dizdaroglu, M. 8,5′-Cyclopurine-2′-deoxynucleosides in DNA: mechanisms of formation, measurement, repair and biological effects. *DNA Repair (Amst)* **2008**, *7*, 1413–1425.
(29) Chatgilialoglu, C.; Ferreri, C.; Terzidis, M. A. Purine 5′,8-cyclonucleoside lesions: chemistry and biology. *Chem. Soc. Rev.* **2011**, *40*, 1368–1382.
(30) Kant, M.; Jaruga, P.; Coskun, E.; Ward, S.; Stark, A. D.; Baumann, T.; Becker, A. A.; Adhikary, A.; Sevilla, M. D.; Dizdaroglu, M. Ion-Beam Radiation Damage to DNA: From Initial Free Radical Formation to Resulting DNA-Base Damage. *ACS Omega* **2021**, *6*, 16600–16611.
(31) Cadet, J.; Wagner, J. R. DNA base damage by reactive oxygen species, oxidizing agents, and UV radiation. *Cold Spring Harb. Perspect. Biol.* **2013**, *5*, No. a012559.
(32) Laurent, Q.; Martinent, R.; Moreau, D.; Winssinger, N.; Sakai, N.; Matile, S. Oligonucleotide Phosphorothioates Enter Cells by Thiol-Mediated Uptake. *Angew. Chem.* **2021**, *133*, 19250–19254.
(33) Clavé, G.; Reverte, M.; Vasseur, J.-J.; Smietana, M. Modified internucleoside linkages for nuclease-resistant oligonucleotides. *RSC Chem. Biol.* **2021**, *2*, 94–150.
(34) Eckstein, F. Phosphorothioates, Essential Components of Therapeutic Oligonucleotides. *Nucleic Acid Ther.* **2014**, *24*, 374–387.
(35) Wang, L.; Jiang, S.; Deng, Z.; Dedon, P. C.; Chen, S. DNA phosphorothioate modification-a new multi-functional epigenetic system in bacteria. *FEMS Microbiol. Rev.* **2019**, *43*, 109–122.
(36) Eckstein, F. Phosphorothioation of DNA in bacteria. *Nat. Chem. Biol.* **2007**, *3*, 689–690.
(37) Stec, W. J.; Grajkowski, A.; Kobylanska, A.; Karwowski, B.; Koziolkiewicz, M.; Misiura, K.; Okruszek, A.; Wilk, A.; Guga, P.; Boczkowska, M. Diastereomers of Nucleoside 3′-O-(2-Thio-1,3,2-oxathia(selena)phospholanes): Building Blocks for Stereocontrolled Synthesis of Oligo(nucleoside phosphorothioate)s. *J. Am. Chem. Soc.* **1995**, *117*, 12019–12029.
(38) Baraniak, J.; Kaczmarek, R.; Stec, W. J. Conjugation of Amino Acid O-Methyl Esters With AZT-5′-O-Phosphorothioate and Phosphorodithioate. *Tetrahedron Lett.* **2000**, *41*, 9139–9142.
(39) Baraniak, J.; Kaczmarek, R.; Wasilewska, E.; Stec, W. J. Oxathiaphospholane Approach to the Synthesis of Conjugates of Amino Acids Methyl Esters with Nucleosides. *Phosphorus Sulfur Silicon Relat. Elem.* **2002**, *177*, 1667–1670.
(40) Baraniak, J.; Kaczmarek, R.; Korczyński, D.; Wasilewska, E. Oxathiaphospholane Approach to N- and O-Phosphorothioylation of Amino Acids. *J. Org. Chem.* **2002**, *67*, 7267–7274.
(41) Zhdanov, R. I.; Zhenodarova, S. M. Chemical Methods of Oligonucleotide Synthesis. *Synthesis* **1975**, *1975*, 222–245.
(42) Martynov, I. V.; Kruglyak, Y. L.; Leibovskaya, G. A.; Khromova, Z. I.; Strukov, O. G. Phosphorylated Oximes. IV. Reactions of 1,3,2-Dioxa- and 1,3,2-Oxathiaphospholanes With α-Halonitrosoalkanes. *Zh. Obshch. Khim 39*, 996–999. *J. Gen. Chem. USSR* **1969**, *1969*, 966–969.
(43) Peake, S. C.; Fild, M.; Schmutzler, R.; Harris, R. K.; Nichols, J. M.; Rees, R. G. Preparation and Nuclear Magnetic Resonance Spectral Analysis of Some 1,3,2-Dithiaphospholans. *J. Chem. Soc. Perkin Trans.* **1972**, *2*, 380–385.
(44) Kamer, P. C. J.; Roelen, H. C. P. F.; van den Elst, H.; van der Marel, G. A.; van Boom, J. H. An Efficient Approach Toward the Synthesis of Phosphorothioate Diesters Via the Schönberg Reaction. *Tetrahedron Lett.* **1989**, *30*, 6757–6760.
(45) Khanduri, D.; Adhikary, A.; Sevilla, M. D. Highly Oxidizing Excited States of One-Electron Oxidized Guanine in DNA: Wavelength and pH Dependence. *J. Am. Chem. Soc.* **2011**, *133*, 4527–4537.
(46) Adhikary, A.; Khanduri, D.; Sevilla, M. D. Direct observation of the protonation state and hole localization site in DNA-oligomers. *J. Am. Chem. Soc.* **2009**, *131*, 8614–8619.
(47) Adhikary, A.; Kumar, A.; Munafo, S. A.; Khanduri, D.; Sevilla, M. D. Prototropic Equilibria in DNA Containing One-electron Oxidized GC: Intra-duplex vs. Duplex to Solvent Deprotonation. *Phys. Chem. Chem. Phys.* **2010**, *12*, 5353–5368.
(48) Adhikary, A.; Collins, S.; Khanduri, D.; Sevilla, M. D. Sugar radicals formed by photo-excitation of guanine cation radical in oligonucleotides. *J. Phys. Chem. B* **2007**, *111*, 7415–7421.
(49) Jie, J.; Xia, Y.; Huang, C. H.; Zhao, H.; Yang, C.; Liu, K.; Song, D.; Zhu, B. Z.; Su, H. Sulfur-centered hemi-bond radicals as active intermediates in S-DNA phosphorothioate oxidation. *Nucleic Acids Res.* **2019**, *47*, 11514–11526.
(50) von Sonntag, C. *Free-Radical-Induced DNA Damage and Its Repair*; Springer-Verlag: Berlin, Heidelberg, 2006, 419–426.
(51) Adhikary, A.; Bothe, E.; Jain, V.; von Sonntag, C. Pulse radiolysis of the DNA-binding ligands Hoechst 33258 and 33342 in aqueous solution. *Int. J. Radiat. Biol.* **2000**, *76*, 1157–1166.
(52) Wojnárovits, L.; Takács, E. Rate constants of dichloride radical anion reactions with molecules of environmental interest in aqueous solution: a review. *Environ. Sci. Pollut. Res.* **2021**, *28*, 41552–41575.
(53) Buxton, G. V.; Bydder, M.; Salmon, G. A. Reactivity of chlorine atoms in aqueous solution Part 1. The equilibrium $Cl^{\bullet} + Cl^{-} \rightleftharpoons Cl_2^{\bullet-}$. *J. Chem. Soc. Faraday Trans.* **1988**, *94*, 653–657.
(54) Navaratnam, S.; Parsons, B. J.; Swallow, A. J. Some Reactions of the Dichloride Anion Radical. *Radiat. Phys. Chem.* **1980**, *15*, 159–161.
(55) Buxton, G. V.; Greenstock, C. L.; Helman, W. P.; Ross, A. B. Critical review of rate constants for reactions of hydrated electrons, hydrogen atoms and hydroxyl radicals ($^{\bullet}OH/O^{\bullet-}$) in aqueous solution. *J. Phys. Chem. Ref. Data* **1988**, *17*, 513–886.
(56) Alfassi, Z. B.; Schuler, R. H. Reaction of azide radicals with aromatic compounds. Azide as a selective oxidant. *J. Phys. Chem.* **1985**, *89*, 3359–3363.
(57) Wojnárovits, L.; Takács, E. Rate constants of sulfate radical anion reactions with organic molecules: A review. *Chemosphere* **2019**, *220*, 1014–1032.
(58) Hasegawa, K.; Neta, P. Rate Constants and Mechanisms of Reaction of $Cl_2^{\bullet-}$ Radicals. *J. Phys. Chem.* **1978**, *82*, 854–857.
(59) Yankova, T. S.; Chumakova, N. A.; Vorob'ev, A. K. Photoinduced orientational order of dichloride anion radicals. *Russ. J. Phys. Chem.* **2011**, *85*, 695–701.
(60) Wardman, P. Reduction potentials of one-electron couples involving free radicals in aqueous solution. *J. Phys. Chem. Ref. Data* **1989**, *18*, 1637–1755.
(61) Armstrong, D. A.; Huie, R. E.; Koppenol, W. H.; Lymar, S. V.; Merényi, G.; Neta, P.; Ruscic, B.; Stanbury, D. M.; Steenken, S.; Wardman, P. Standard electrode potentials involving radicals in aqueous solution: inorganic radicals. (IUPAC Technical Report). *Pure Appl. Chem.* **2015**, *87*, 1139–1150.

https://doi.org/10.1021/acs.jpcb.1c09068
J. Phys. Chem. B 2022, 126, 430–442

(62) Halliwell, B.; Adhikary, A.; Dingfelder, M.; Dizdaroglu, M. Hydroxyl radical is a significant player in oxidative DNA damage *in vivo*. *Chem. Soc. Rev.* **2021**, *50*, 8355−8360.
(63) Buettner, G. The Pecking Order of Free Radicals and Antioxidants: Lipid Peroxidation, α-Tocopherol, and Ascorbate. *Arch. Biochem. Biophys.* **1993**, *300*, 535−543.
(64) Steenken, S.; Jovanovic, S. V. How Easily Oxidizable Is DNA? One-Electron Reduction Potentials of Adenosine and Guanosine Radicals in Aqueous Solution. *J. Am. Chem. Soc.* **1997**, *119*, 617−618.
(65) Seidel, C. A. M.; Schulz, A.; Sauer, M. H. M. Nucleobase-Specific Quenching of Fluorescent Dyes. 1. Nucleobase One-Electron Redox Potentials and Their Correlation with Static and Dynamic Quenching Efficiencies. *J. Phys. Chem.* **1996**, *100*, 5541−5553.
(66) Adhikary, A.; Kumar, A.; Becker, D.; Sevilla, M. D. The Guanine Cation Radical: Investigation of Deprotonation States by ESR and DFT. *J. Phys. Chem. B* **2006**, *110*, 24171−24180.
(67) Candeias, L. P.; Steenken, S. Structure and Acid-Base Properties of One-Electron-Oxidized Deoxyguanosine, Guanosine, and 1-Methylguanosine. *J. Am. Chem. Soc.* **1989**, *111*, 1094−1099.
(68) O'Neill, P.; Davies, S. E. Pulse radiolytic study of the interaction of $SO_4^{\bullet-}$ with deoxynucleosides. Possible implications for direct energy deposition. *Int. J. Radiat. Biol. Relat. Stud. Phys. Chem. Med.* **1987**, *52*, 577−587.
(69) Kobayashi, K.; Tagawa, S. Direct Observation of Guanine Radical Cation Deprotonation in Duplex DNA Using Pulse Radiolysis. *J. Am. Chem. Soc.* **2003**, *125*, 10213−10218.
(70) Zhang, X.; Jie, J.; Song, D.; Su, H. Deprotonation of Guanine Radical Cation $G^{\bullet+}$ Mediated by the Protonated Water Cluster. *J. Phys. Chem. A* **2020**, *124*, 6076−6083.
(71) Candeias, L.; Steenken, S. Reaction of $HO^{\bullet}$ with Guanine Derivatives in Aqueous Solution: Formation of Two Different Redox-Active OH-Adduct Radicals and Their Unimolecular Transformation Reactions. Properties of $G(-H)^{\bullet}$. *Chem. − Eur. J.* **2000**, *6*, 475−484.
(72) Shinde, S. S.; Maroz, A.; Hay, M. P.; Anderson, R. F. One-Electron Reduction Potential of the Neutral Guanyl Radical in the GC Base Pair of Duplex DNA. *J. Am. Chem. Soc.* **2009**, *131*, 5203−5207.
(73) Rokhlenko, Y.; Cadet, J.; Geacintov, N. E.; Shafirovich, V. Mechanistic Aspects of Hydration of Guanine Radical Cations in DNA. *J. Am. Chem. Soc.* **2014**, *136*, 5956−5962.
(74) Shukla, L. I.; Adhikary, A.; Pazdro, R.; Becker, D.; Sevilla, M. D. Formation of 8-oxo-7,8-dihydroguanine-radicals in γ-irradiated DNA by multiple one-electron oxidations. *Nucleic Acids Res.* **2004**, *32*, 6565−6574.
(75) Dizdaroglu, M.; Jaruga, P. Mechanisms of free radical-induced damage to DNA. *Free Radic. Res.* **2012**, *46*, 382−419.
(76) Denisov, V. P.; Carlström, G.; Venu, K.; Halle, B. Kinetics of DNA hydration. *J. Mol. Biol.* **1997**, *268*, 118−136.
(77) Saenger, W. Structure and Dynamics of Water Surrounding Biomolecules. *Ann. Rev. Biophys. Biophys. Chem.* **1987**, *16*, 93−114.
(78) Cao, F.; Ju, X.; Chen, D.; Jiang, L.; Zhu, X.; Qing, S.; Fang, F.; Shen, Y.; Jia, Z.; Zhang, H. Phosphorothioate-modified antisense oligonucleotides against human telomerase reverse transcriptase sensitize cancer cells to radiotherapy. *Mol. Med. Rep.* **2017**, *16*, 2089−2094.

NOTE ADDED AFTER ASAP PUBLICATION

This paper published ASAP on January 6, 2022 with errors (due to production) in eqs 6, 8, and 16. The errors were corrected and the revised paper was republished when the issue published on January 20, 2022.

https://doi.org/10.1021/acs.jpcb.1c09068
J. Phys. Chem. B 2022, 126, 430−442